Climate Dynamics (2005)
DOI 10.1007/s00382-005-0064-x

François Lott · Laurent Fairhead · Frederic Hourdin
Phu Levan

# The stratospheric version of LMDz: dynamical climatologies, arctic oscillation, and impact on the surface climate

Received: 9 December 2004 / Accepted: 18 July 2005


**Abstract** A climatology of the stratosphere is determined from a 20-year integration with the stratospheric version of the Atmospheric General Circulation Model LMDz. The model has an upper boundary at near 65 km, uses a Doppler spread non-orographic gravity waves drag parameterization and a subgrid-scale orography parameterization. It also has a Rayleigh damping layer for resolved waves only (not the zonal mean flow) over the top 5 km. This paper describes the basic features of the model and some aspects of its radiative-dynamical climatology. Standard first order diagnostics are presented but some emphasis is given to the model's ability to reproduce the low frequency variability of the stratosphere in the winter northern hemisphere. In this model, the stratospheric variability is dominated at each altitudes by patterns which have some similarities with the arctic oscillation (AO). For those patterns, the signal sometimes descends from the stratosphere to the troposphere. In an experiment where the parameterized orographic gravity waves that reach the stratosphere are exaggerated, the model stratosphere in the NH presents much less variability. Although the stratospheric variability is still dominated by patterns that resemble to the AO, the downward influence of the stratosphere along these patterns is near entirely lost. In the same time, the persistence of the surface AO decreases, which is consistent with the picture that this persistence is linked to the descent of the AO signal from the stratosphere to the troposphere. A comparison between the stratospheric version of the model, and its routinely used tropospheric version is also done. It shows that the introduction of the stratosphere in a model that already has a realistic AO persistence can lead to overestimate the actual influence of the stratospheric dynamics onto the surface AO. Although this result is certainly model dependent, it suggests that the introduction of the stratosphere in a GCM also call for a new adjustment of the model parameters that affect the tropospheric variability.

F. Lott (✉) · P. Levan
Laboratoire de Météorologie Dynamique, IPSL,
Ecole Normale Supérieure, 24 rue Lhomond,
75235 Paris, Cédex 05, France
E-mail: flott@lmd.ens.fr
Tel.: +33-1-44322752
Fax: +33-1-43368392

L. Fairhead · F. Hourdin
Laboratoire de Météorologie Dynamique, IPSL,
Université Pierre et Marie Curie, boite 99, 4 place Jussieu,
75252 Paris, Cédex 05, France

## 1 Introduction

LMDz is the atmospheric general circulation model developed at the Laboratoire de Météorologie Dynamique. It is essentially used for climate prediction and does not extend up beyond the lower stratosphere, where it has a strongly degraded vertical resolution. Here we report the first results from a multi-year integration of a troposphere–stratosphere configuration of this model, document its simulation of the arctic oscillation (AO), and analyze the impact of its stratosphere on its surface climate.

Following the Geophysical Fluid Dynamics Laboratory (GFDL) "SKYHI"GCM (Fels et al. 1980) most research groups involved in climate simulation have included the middle atmosphere in their GCMs (Hamilton et al. 1995; Rind et al. 1988; Boville 1995; Beagley et al. 1997; Butchart and Austin 1998; Manzini et al. 1997; Langematz and Pawson 1997; Déqué et al. 1994). The principal motivation behind these developments is the simulation of the chemical climate, the middle atmosphere being a region where dynamics, chemistry and radiation play equal roles and interact strongly with each other (Andrews et al. 1987). For this purpose, a first natural step is the development of a dynamical model where the radiatively active chemical species are imposed via climatologies.

A second motivation is purely dynamical, and is related to a series of papers starting from the late 90s, and which have shown that the mid-latitude stratospheric low-frequency variability precedes sometime the tropospheric one. This downward influence concerns near zonally symmetric patterns like the AO (Baldwin and Dunkerton 1999) as well as planetary waves (Perlwitz and Harnick 2003). Although most of the related research initially relies on reanalysis datasets, these results have been supported by idealized model studies (Polvani and Kushner 2002; Song and Robinson 2004) and there are more and more studies that address this problem in realistic GCMs. Christiansen (2001) for instance, showed that the ARPEGE GCM (Déqué et al. 1994) can produce downward propagations of zonal-mean wind anomalies. Boville (1984) and Norton (2003) have shown that the stratosphere affects substantially the tropospheric variability by comparing GCMs experiments where the stratosphere is dynamically active to experiments in which the stratospheric variability is substantially degraded.

The first objective of the present work is to establish the strengths and weaknesses of the troposphere–stratosphere configuration of LMDz for future chemistry and climate studies. In this paper we concentrate on the model's climatology in the extratropics and on its low-frequency variability. We also examine the model's ability to reproduce the AO, that is the correct large-scale dynamical conditions for the dynamics in the stratosphere to influence the low frequency variability in the troposphere.

A second objective of this paper is to give further evidence that the dynamics of the stratosphere increase the predictive skill of the surface AO. For this, we follow Norton (2003) and Boville (1984) and present an experiment where the stratospheric variability is artificially decreased. To do this, a different method with respect to those used by these authors is employed. Instead of increasing the damping of the large scale patterns directly, via enhanced stratospheric diffusion as in Boville (1984) or enhanced Rayleigh friction as in Norton (2003), we exaggerate the amount of parameterized orographic gravity waves (OGWs) that reach the stratosphere. In doing this, we nevertheless choose parameters in the OGWs scheme such the interannual low frequency variability stays dominated at all altitudes by AO-like patterns that are near those in the control run. In this context, the degraded experiment permits to analyze if the descent of the AO from the stratosphere to the troposphere is an important dynamical mechanism that links these two domains at low frequency. More specifically, if this descent is not affected substantially in the degraded run, and if the surface persistence of the AO is, the relationships between the stratospheric dynamics and the surface climate is more a question of amplitude and timescale of the stratospheric variability than of propagation of the AO signal from the stratosphere to the troposphere.

To a certain extent, this comparison between two simulations with very different stratospheric dynamics can also be viewed as a validation of our model. Indeed, as comparable exercises have been done already with other models, it is worthwhile to analyse if our model presents comparable sensitivities of the surface climate to the stratospheric dynamics.

The plan of the paper is as follows. Section 2 presents a description of the model and of the observational datasets that are used for comparison. Section 3 presents standard monthly mean fields and diagnostics of the meridional circulation. Section 4 presents the model variability in the troposhere and in the stratosphere. Section 5 documents its simulation of the AO. Section 6 documents the sensitivity of the model surface climate to the model stratospheric variability. In it, the dynamical behavior of the model is evaluated comparing the simulation documented in Sects. 2, 3, 4, and 5 to a simulation with degraded stratospheric dynamics and to a simulation without stratosphere. Section 7 concludes.

## 2 Model description and experiments set-up

The model used is an upward extension of the LMDz fourth-generation atmospheric GCM. Some elements of its structure and tropospheric climatologies can be found in Lott (1999) for the midlatitudes, and in Li (1999) for the tropics. Its tropospheric version is largely used in the French Research community (Hourdin et al. 2002; Krinner and Genthon 2003; Bony et al. 2004; Quaas et al. 2004; Reddy and Boucher 2004, among others) and starts to include interactive chemistry (for the troposphere, see Hauglustaine et al. 2004).

It is a gridpoint model in the horizontal direction, the equations being discretized on a staggered latitude–longitude Arakawa-C grid. It currently uses a uniform resolution of 2.5° in latitude and 3.75° in longitude. The vertical resolution is in term of an hybrid sigma pressure vertical coordinate where the model level pressure $P_n = A_n + B_n P_s$. The $B_n$ values are near 0 above the log-pressure altitude of 13 km, ensuring pure pressure vertical coordinates in the stratosphere. The $A_n$ values are such that the upper level is near 65 km, that the resolution in the stratosphere varies slowly from 1 km at $z = 12$ km to 3 km at $z = 50$ km and reaches 6 km at the model top. Although many models go beyond this altitude, our choice here is a compromise that permits to have a refine resolution near and above the tropopause and a well resolved stratosphere at a reasonable computational cost. Nevertheless, versions of the model that include the entire middle atmosphere are currently tested. Other salient features of the dynamical core of the model are: a discretization on an Arakawa-C grid that ensures numerical conservation of barotropic enstrophy (Sadourny 1975); Fourier filtering in polar latitudes to eliminate undesirable restrictions on the choice of time step; and horizontal diffusion on model levels of the

form $\left(\vec{\nabla}.K\vec{\nabla}\right)^n$ to remove unwanted grid-scale noise. For the integrations reported here the values for the horizontal diffusion parameters $n=2$ and $K$ are such that the smallest (grid-) scales have a dissipation time-scale of 1 h. Although these values can lead to rather large diffusion for relatively large wavelengths, they are needed in LMDz because the numerical diffusion of the horizontal discretization scheme is very small. The time step equals 3 min, a value imposed by the entirely explicit treatment of the dynamical tendencies.

The salient features of the physical parameterizations used in the model are briefly summarized here: the radiation scheme is based on the ECMWF scheme (Morcrette 1991), the convection scheme is based on Tiedtke (1989), and the turbulent mixing in the planetary boundary layer is based on a local second order closure formalism. On top of these conventional parameterizations, the subgrid scale orography (SSO, which forces orographic gravity waves) is represented following Lott and Miller (1997) and Lott (1999). Compared to the tropospheric version in Lott (1999), the parameters of the SSO scheme that control the amount of gravity waves that propagate toward the middle atmosphere have been slightly modified. In particular, the nondimensional parameter that tunes the gravity wave stress amplitude has been decreased to $G=0.2$ (instead of $G=1$ in Lott 1999), and only 10% of the surface gravity waves stress is transmitted to the upper atmosphere ($\beta=0.9$ instead of 0.5 in Lott (1999)). The stratospheric version of LMDz also includes a Doppler-spread non-OGWs scheme based on Hines (1997a, b) and adapted from Manzini et al. (1997). In it, the launching altitude for the gravity waves is the model ground, and the constant gravity wave RMS wind speed is 1 m/s. The stratospheric version of LMDz also includes a Rayleigh drag sponge layer between 55 and 65 km that damps the resolved waves and not the mean-flow (Shepherd et al. 1996).

The model results presented are from three 20 year integrations forced at the lower boundary by SSTs and sea-ice cover that vary along a climatological annual cycle. The ozone also varies along a climatological annual cycle, and using smooth analytical functions varying with latitude time and pressure. The parameters of the functions have been adjusted for that the difference between our climatology and the Fortuin and Kelder (1998) climatology is below 1 ppmv at all times, latitude and altitudes below 50 km. Note that in none of the simulations presented the model generate a QBO in the lower tropical stratosphere.

To validate our model, we will essentially use 20 years (1981–2000) of the ERA40 ECMWF analysis (Simmons and Gibson 2000). For the monthly mean fields in Sect. 3.1, we will also use the CIRA dataset (Fleming et al. 1990) because the ECMWF reanalysis does not extent above 50 km, while our model does. Although there is essentially a damping layer in the model there, a brief check is needed there for future runs with chemistry, and to control for instance that the model temperatures are not out of range there.

## 3 Monthly mean fields

### 3.1 Zonal wind and temperature

In this section monthly mean fields for the 20-year reference run are presented for the four cardinal months January, April, July, and October. Note that we have chosen here and in the next subsection to present the model fields up to the model top, and despite the fact that a good part of our low mesosphere is occupied by an artificial sponge layer. Figure 1 shows the zonal mean temperature from the model. It shows a well defined mid-latitude tropopause around 10 km, and a temperature minimum in the vertical around 16 km in the tropics, a local temperature minimum in the winter polar lower stratosphere, and a well defined stratopause around 50 km. At this level, the temperature is maximum in the vertical for all latitudes and seasons, and the pole to pole meridional temperature gradient reverses during solstice seasons, presenting a local maximum at the summertime polar stratopause.

Although these features agree qualitatively with the observations, some pronounced model biases can be seen, when comparing with the CIRA climatology in Fig. 2. The low mesosphere is near everywhere too cold and there is a warm bias around 5–10 K at the summer polar stratopause during solstices (around 50 km). The polar winter stratosphere is typically 5 K too cold and the equatorial lower stratosphere (between 20 and 30 km) is also 5 to 10 K too cold during all seasons. Note as well that during solstices, the stratopause altitude (e.g. the maximum in T around 50 km) does not vary as much with latitude as it does in the CIRA dataset. Note also that the minimum temperature at the tropical tropopause (e.g. around 16 km) is around 200 K, it is warmer than in the CIRA climatology. As this value is critical for the injection of water vapor in the stratosphere, we have examined the evolution of the zonal mean T at 16 km and compared it to that from the ECMWF reanalysis (not shown). In the model, the 16 km mean temperature at the equator never goes below 196 K while in the reanalysis it goes below 192 K, indicating a warm bias of near 5 K there.

Figure 3 shows the zonal mean zonal wind from the model. Again these features agree qualitatively with observations, and the biases are usually those found in other models (see for instance, Pawson et al. 2000). In the midlatitudes, they essentially result from the biases seen in the temperature. For instance, the cold bias in stratospheric temperature in the polar southern Hemisphere, translates into a westerly bias of 5–10 m/s in the polar vortex in July (between 20 and 30 km). This westerly bias is even more pronounced at the stratopause. It is also present in April, and is even more pronounced in

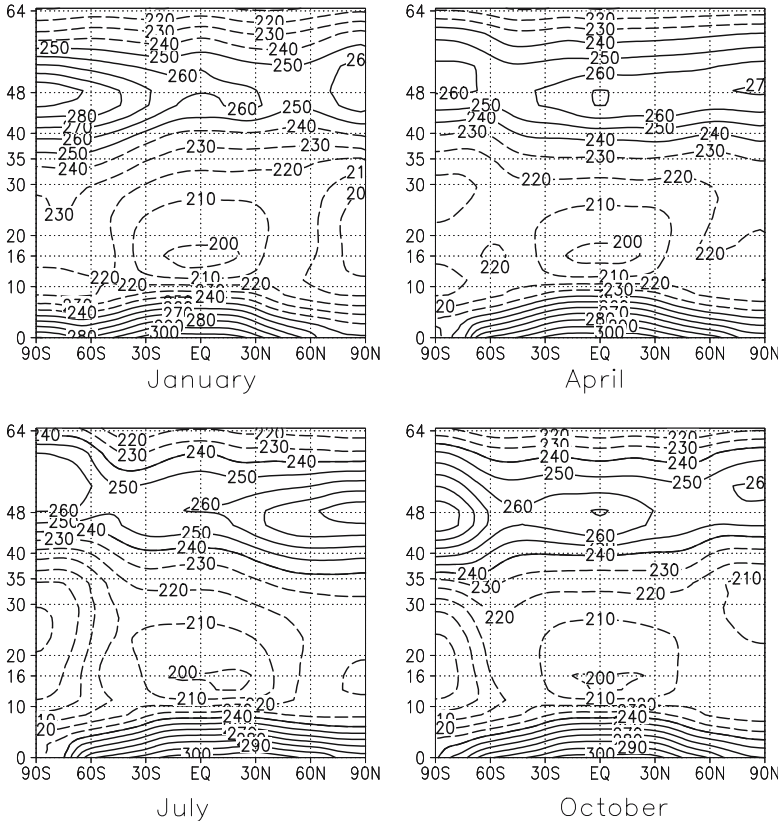


**Fig. 1** Zonally averaged temperature fields in Kelvin, calculated from a 20-year run with the LMDz model. Contour interval = 10 K, values below 250 K *dashed*

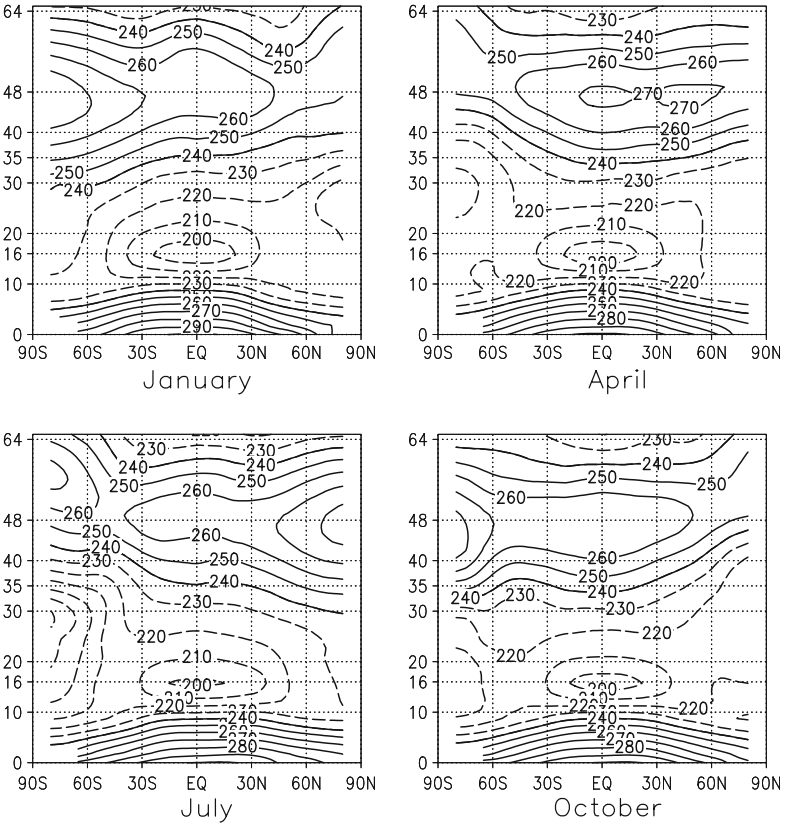


**Fig. 2** Same as Fig. 1 but from the CIRA climatology

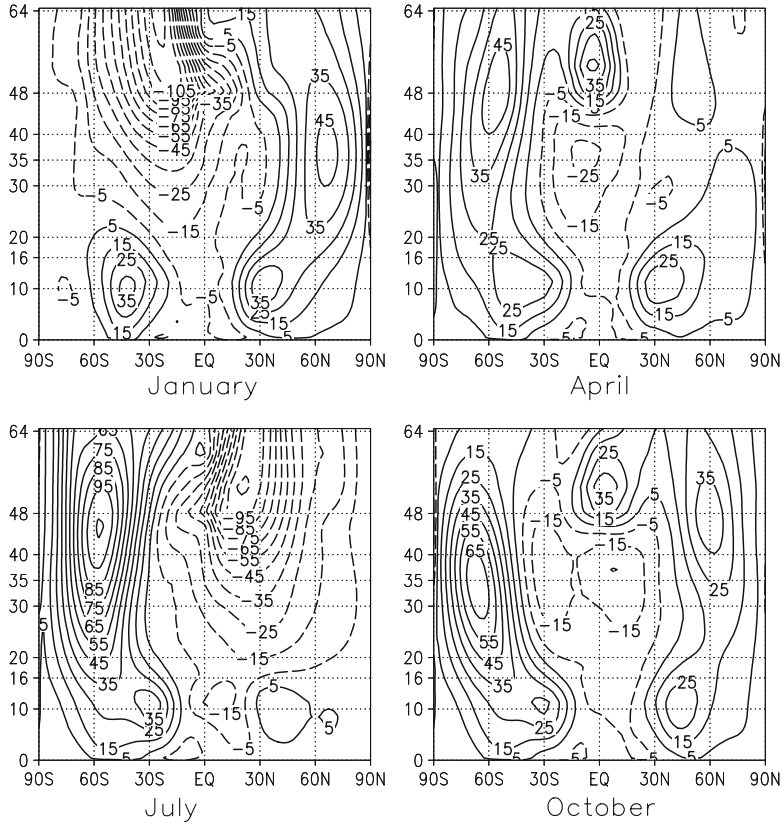


**Fig. 3** Zonally averaged zonal wind fields in m/s, calculated from a 20-year run with the LMDz model. Contour interval = 10 m/s. Negative values are *dashed*

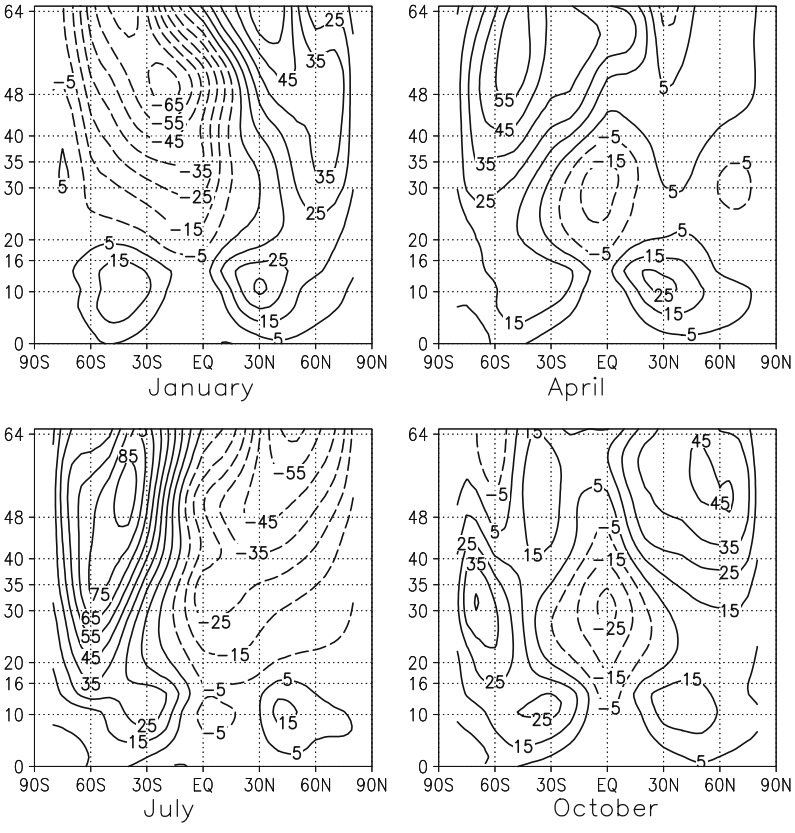


**Fig. 4** Same as Fig. 3 but for the CIRA climatology

October. In the northern hemisphere, comparable biases can be found with a 10 m/s too strong polar vortex in the entire stratosphere. Near the model top, in the lower mesosphere, the westerlies tilt toward the equator, a result due to the GWs parameterizations (Manzini et al. 1997). Note also that the summer easterlies in the mid-latitudes and subtropics have a strong negative bias in the upper stratosphere and in the low mesosphere (i.e. for $z > 35$ km). This bias may follow that the launch altitude of the Doppler spread gravity waves parameterization scheme is the ground. In that circumstance, Manzini and McFarlane (1998) have shown that the GWs momentum flux at the tropopause is negative, a process that limits the upper mesospheric acceleration of the easterlies. In our model though, the error is near 40 m/s in the easterlies of the lower mesosphere subtropics, it is likely that the effect of the Doppler spread parameterization is not the only cause of this. Note as well that another substantial error is found in the lower equatorial mesosphere, where a stronger than usual semi annual oscillation modulates the velocity field in April and October.

### 3.2 Meridional circulation

The mean meridional circulation provides the link between radiative heating and dynamical forcing. It is examined here in the framework of the transformed Eulerian mean formalism (Andrews et al. 1987), where the residual meridional velocity $\overline{v}^*$ differs from the zonal mean Eulerian meridional velocity $\overline{v}$ by:

$$\overline{v}^* = v - \rho_0^{-1}\left(\rho_0^{-1}\overline{v'\theta'}/\overline{\theta}_z\right)_z \quad (1)$$

All notations here are conventional: the overbar denotes a zonal mean, the prime represents deviation from the zonal mean, $z$ is the log-pressure vertical coordinate, $\rho_0(z)$ is a reference density profile, and $\theta$ is the potential temperature. Alternatively, the residual circulation can be represented using a mass streamfunction:

$$\frac{\partial \overline{\Psi}^*}{\partial z} = -\rho_0 \cos(\phi)\overline{v}^* \quad (2)$$

The results from the model are shown in Fig. 5 for $\overline{\Psi}^*$, integrating Eq. 2 from the model top and imposing $\overline{\Psi}^* = 0$ there. As positive contours represent a circulation in the clockwise sense, the model correctly reproduces the Brewer Dobson circulation (see Fig. 6 for the re-analysis). In January and July, the winter cells in the stratosphere are much stronger than the summer cells. They are nevertheless less pronounced than in the reanalysis in Fig. 6. Still in January and July, but at the stratopause and in the low mesosphere, the model also reproduces the summer to winter pole meridional circulation. Note nevertheless, that the model overestimates in July the mesospheric circulation, bringing too much mesospheric air into the winter vortex. During Equinoxes, the model reproduces as well the two cells apparent in both the stratosphere and the mesosphere, with values in better agreement with the reanalysis, compared to during solstices. Note that these behaviors of the residual circulation in the model are rather robust, they are near those in the degraded simulation presented in Sect. 6, and near those from a coupled-chemistry simulation that has been recently made (not shown).

## 4 Planetary waves and variability in the mid-latitudes

### 4.1 Tropospheric climate and variability

Since the middle atmosphere is driven within a good part by planetary waves emanating from the troposphere, a reasonable middle atmosphere climate strongly relies on a reasonable simulation of the troposphere climate and variability. Figure 7a shows the average of the 700 hPa geopotential height (Z700) from the model. It presents two major troughs at the East coasts of America and Asia, and two major ridges over north-eastern America and north-eastern Europe. There is as well a less pronounced trough over Central Europe and a weak ridge to its East (i.e. to the North of the Himalayan plateau). It is noteworthy, that these features are well predicted in the model when compared to the reanalysis. This in part results from the action at low level of the Subgrid Scale Orographic scheme presented in Lott (1999). Nevertheless, when compared to the ECMWF data in Fig. 8a, the model slightly underestimates: the ridge over the Rockies; the diffluence of the jet over western Europe; and the latitudinal extension of the trough over the western Pacific.

The root mean square of Z700 in Fig. 7b, reveals two centers of action, slightly to the west of the two major ridges in Fig. 7a. It is noteworthy that the locations of these two centers of action are very realistic when compared to Fig. 8b. The model nevertheless seems to slightly overestimate the tropospheric variability.

It is a well known result (Sawyer 1976; Blackmon 1976) that the total variance in the atmosphere is dominated by the low-frequency variability, and that it hides the transient eddies resulting from the baroclinic instabilities generated where the midlatitude jet is intense (on the lee side of the two major troughs in Figs. 7a and 8a). To isolate these baroclinic activity we next use the procedure in Hoskins et al. (1989), and define the high pass transient fields by the difference between the daily field and the centered box-car 3-day mean of that field. The rms of this high pass field is presented in Fig. 7c, for the winter NH. The baroclinic storm tracks are located at the two jet exits, with maximum variance over the western half of the two oceans and extension over the entire oceanic basins. Note nevertheless, that over the entire Pacific the model underestimates substantially the high pass rms (Fig. 8c).

For the southern hemisphere winter in Fig. 7d the climatological mean flow is much more zonal. At

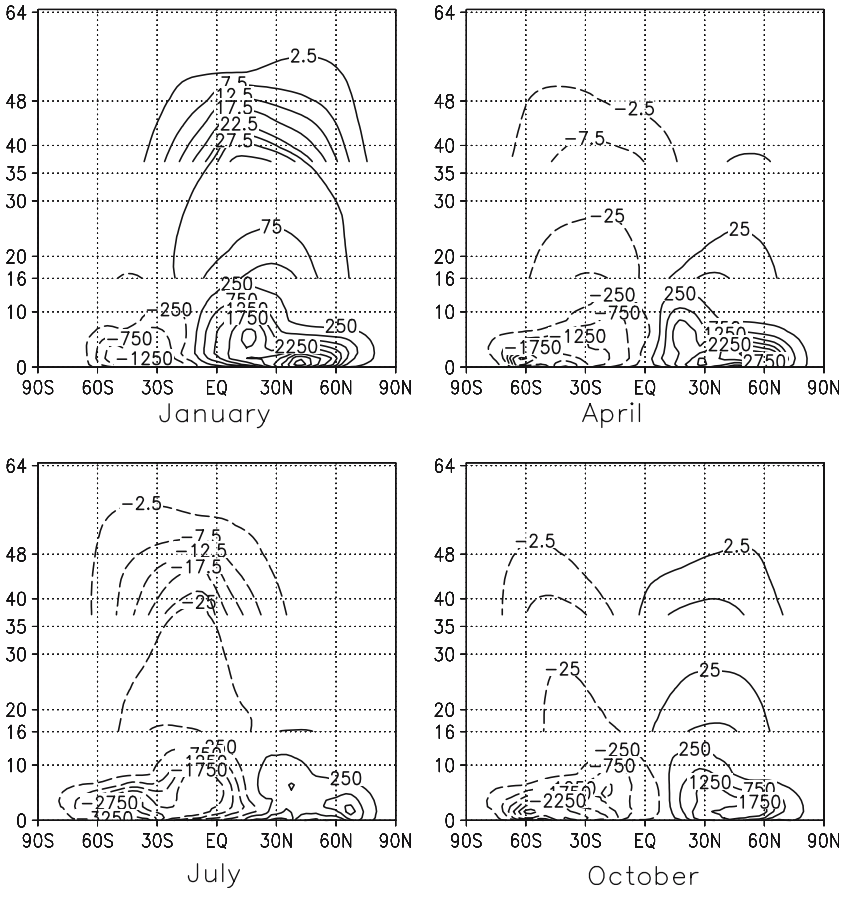


**Fig. 5** Mean residual streamfunction (Eq. 2) from the 20-year model integration, negative values are *dashed*. Contour interval: 500 kg/m/s between 1 and 16 km, 50 kg/m/s between 16 and 37 km, and 5 kg/m/s above 37 km

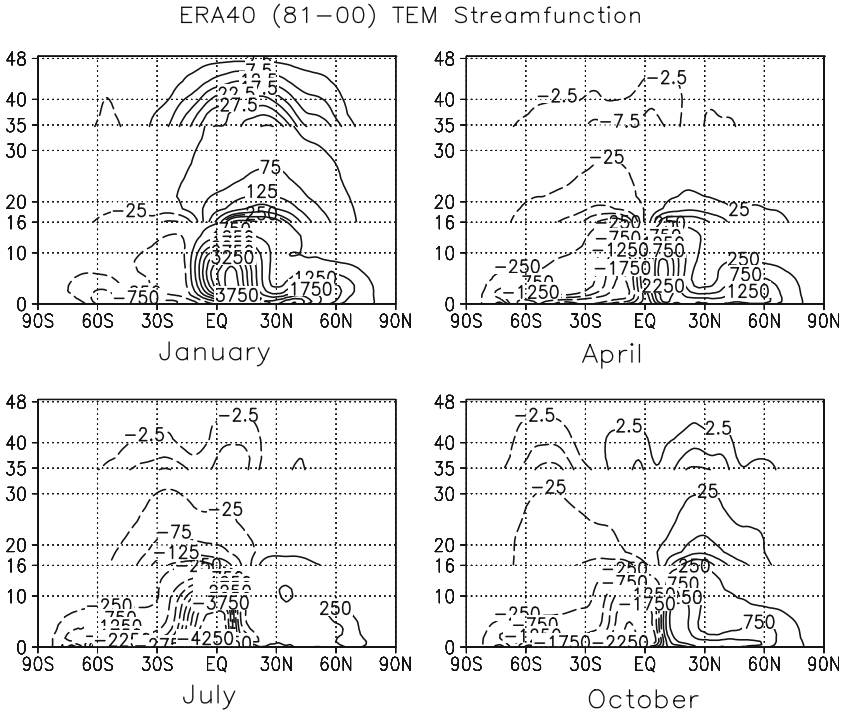


**Fig. 6** Same as Fig. 5 but from the ECMWF reanalysis, and for the years 1980–2000

southern latitudes around 60°S, it presents enhanced variance over near half the globe in latitude, with a maximum over southern east Pacific near the Drake passage (Fig. 7e). The pattern of high frequency in Fig. 7f presents enhanced variance slightly to the north of the maximum of total variance in Fig. 7e. It covers

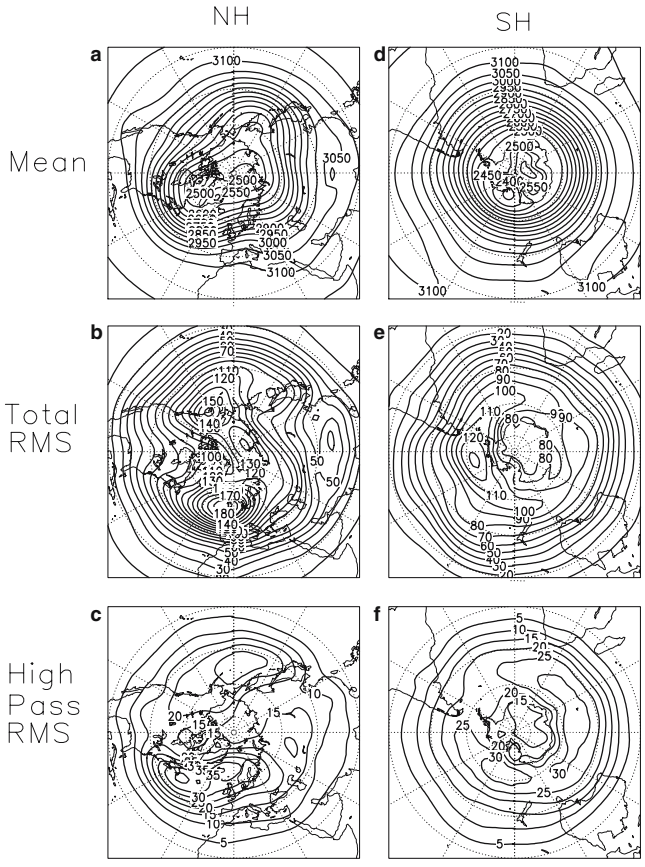


**Fig. 7** DJF statistics of 700 hPa geopotential height for 20 winters and from the LMDz: model. **a–d** Winter mean contour, interval 50 m; **b–e** rms, contour interval 10 m; **c–f** rms high pass, contour interval 5 m

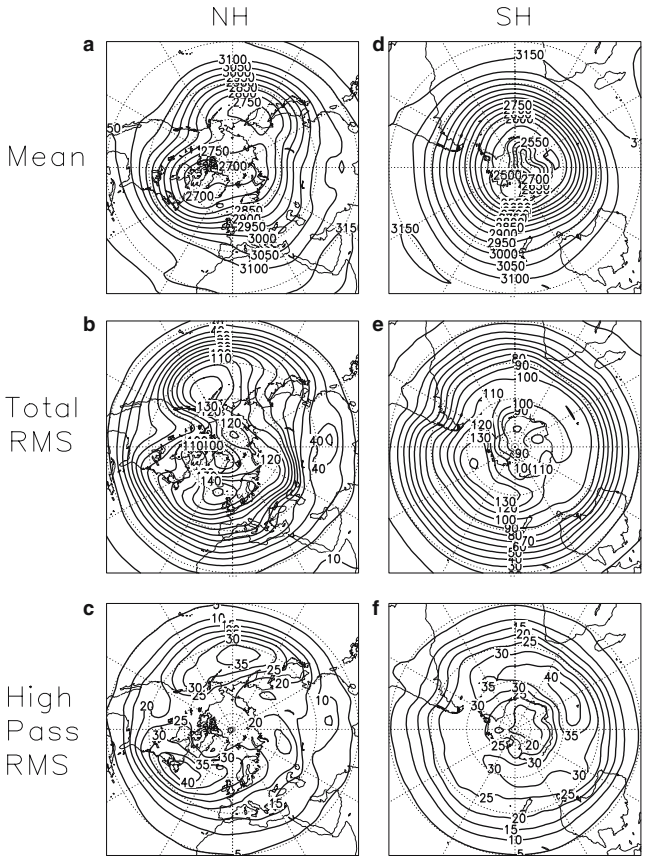


**Fig. 8** Same as Fig. 7 but for the ECMWF reanalysis and for the years 1980–2000

more than half the globe around 50°S, and with a pattern that is near the symmetric with respect to the pole. Again, these patterns are rather realistic, with the model slightly underestimating both the total variance and the high pass variance (see Fig. 8d, e, f for the reanalysis).

## 4.2 Stratospheric planetary waves and zonal mean variability

Most of the stratospheric variability in the NH arises from large-scale perturbations of the polar vortex by upward propagating planetary waves that originate in the troposphere (Charney and Drazin 1961). Accordingly, a good representation of these planetary waves is essential for our stratospheric climate to be reasonable. The January statistics of the first three planetary waves from the model are shown in Fig. 9. The corresponding fields from the reanalysis are shown in Fig. 10.

Overall, it is clear that the rather realistic simulations of the zonal mean fields and tropospheric climate result in the forcing of planetary waves that are both realistic in phase and amplitude. Note nevertheless that the model has a tendency to overestimate the amplitude and variability of the first three planetary waves. Although not shown here for conciseness, the same results hold for other months as well as for the SH. Rather noticeable differences are nevertheless found for the SH in July, with the model overestimating by a factor larger than two the planetary wave number two in the stratosphere, while it underestimates by the same factor the planetary wave number three (not shown).

As a result of the interaction between these planetary waves and the zonal mean flow, the standard deviation of the zonal mean geopotential height fields must present variations that compare as well with those from the reanalysis. For the model and for the four calendar months January, April, July and October, these are displayed in Fig. 11. Figure 11 shows that in the NH high latitudes the model zonal mean geopotential variability is larger during winter and spring, and very small in summer and autumn. This seasonal variation in variability is explained by the tendency of sudden stratospheric warmings to occur in winter and early spring, and agrees well with that in the reanalysis in Fig. 12. In the SH high latitudes, in the model as in the observations, the zonal mean geopotential variability is also large during winter and spring (e.g. July and October).

In order to give a last view of the model's simulation of the mid-latitude stratospheric variability, we next

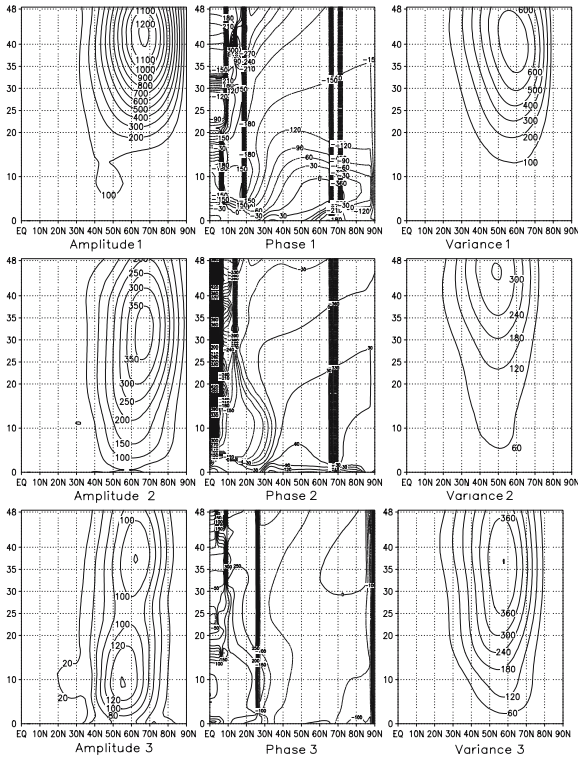


**Fig. 9** January planetary waves diagnostics of geopotential height fields for 20 winters and from the LMDz model. Wave with zonal wavenumber 1: **a** mean amplitude, **b** mean phase, and **c** intra-seasonal standard deviation due to wave 1. Wave with zonal wavenumber 2: **d** mean amplitude, **e** mean phase, and **f** intra-seasonal standard deviation due to wave 2; wave with zonal wavenumber 3: **g** mean amplitude, **h** mean phase, and **i** intra-seasonal standard deviation due to wave 3

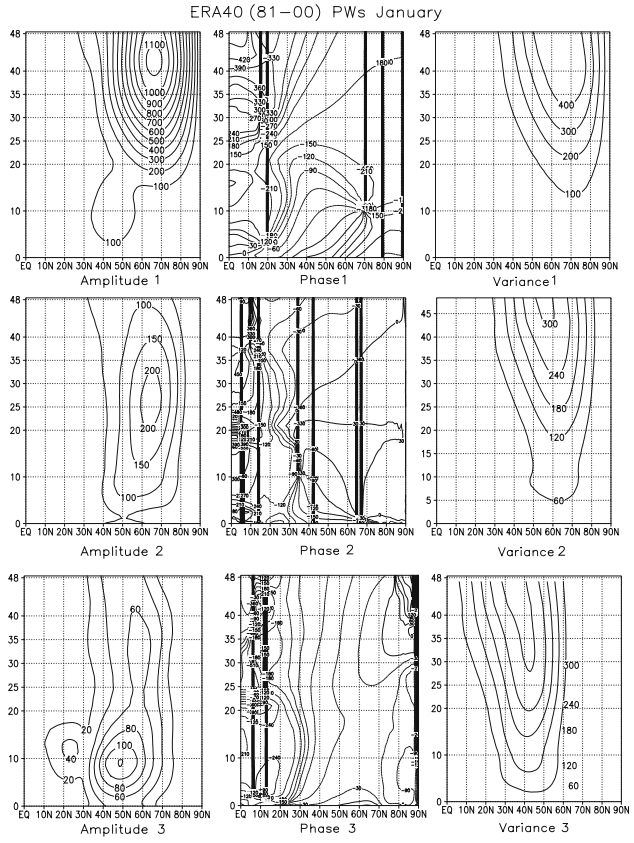


**Fig. 10** Same as Fig. 9 but for the ECMWF reanalysis

present time series of the simulated mid-stratosphere temperatures over the poles in Fig. 13. The figure clearly shows that the model captures the general nature of the temperature variations, their seasonal dependence and the contrasts between the two hemispheres that can be seen in Fig. 14 for the ECMWF reanalysis. However, the model has slight cold biases of near 5 K at both poles. These cold biases are also present in the low stratosphere (e.g. around 50 mb). For instance, there are years where the temperature at the North Pole can be below 190 K during more than a month in late winter. It is also systematically below this value at the South Pole in August and September. For both poles these values are critically too low and it is likely that this version of the model will destroy too much ozone in a coupled climate chemistry simulation.

In addition, the model NH polar temperature displays greater interannual variability from January to April (late winter to early spring) than does the reanalysis. The North Pole time series also show that the model develops stronger and longer lasting warmings than in the reanalysis. The interannual variability in the timing also shows that the warmings in the model never happen in December, in contradiction with the reanalysis. May be the small warmings that occur in two occasions in November, e.g. too early in winter, prevents the model to develop substantial warmings in December. Figure 13a also shows that the warmings in the model occur throughout the winter, and that the vortex can reconstruct after a warming simulated between January and February. The variability in the South Pole temperature at 10 hPa is realistic as well, with the difference between the years much smaller than for the North Pole. The South Pole time series shows no significant warming, except may be in spring.

## 5 Propagation of the AO

To analyze the dynamical links between the stratosphere and the troposphere in our model, we follow Baldwin and Dunkerton (1999) and adopt the viewpoint that the AO is the largest and most fundamental mode of variability in the troposphere–stratosphere system. Nevertheless, our approach differs somehow from their, in the sense that we apply empirical orthogonal function analysis (EOF, Preisendorfer 1988) level by level rather than globally. Note that our technique applied to the reanalysis data gives result that are consistent with theirs. This follows that in the data and models, the AO is sufficiently robust to be recovered using variety of techniques and data levels.

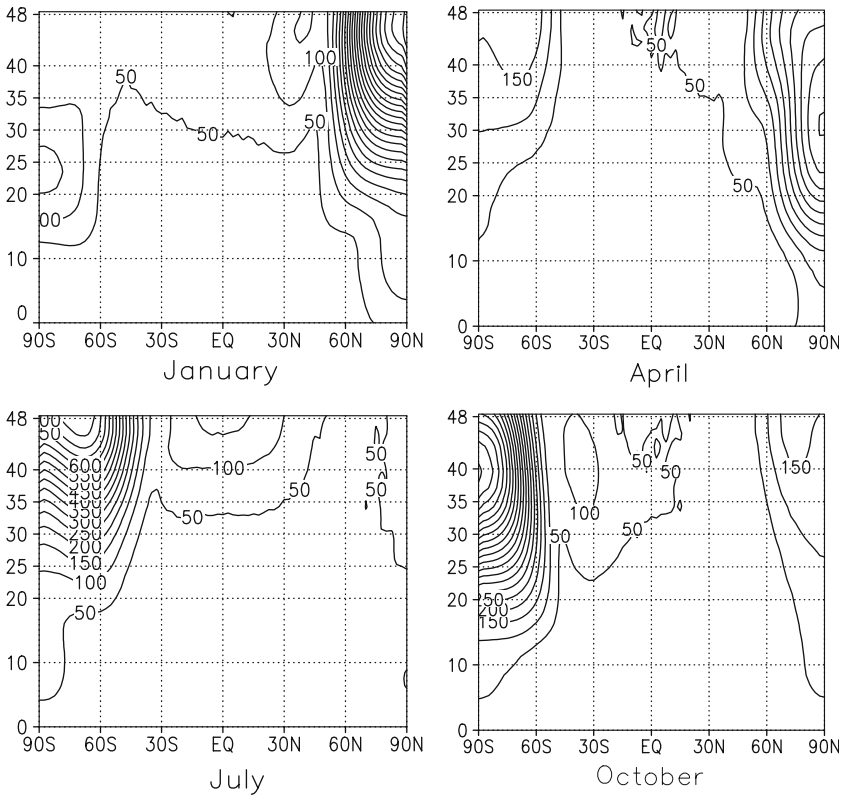


**Fig. 11** Standard deviation of the zonal mean geopotential height from the model during the four calendar months, January, April, July, and October. Contour: 50 m

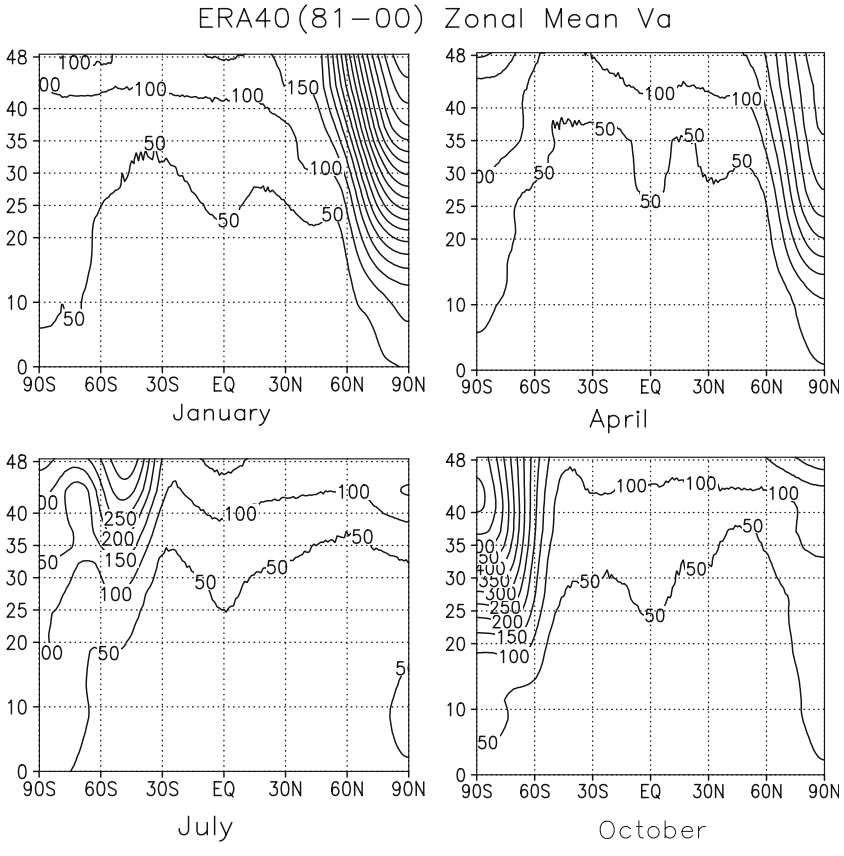


**Fig. 12** Same as Fig. 11 but for the ECMWF reanalysis

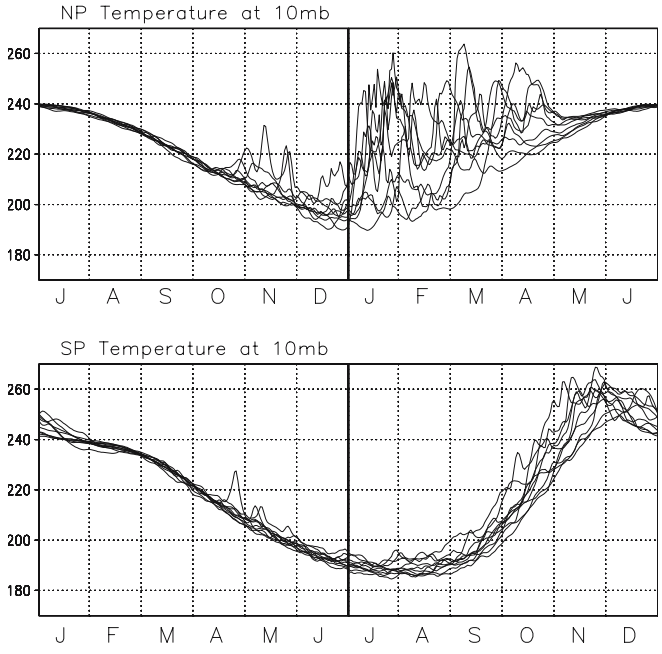


**Fig. 13** Polar temperatures at 10 hPa in LMDz and for 10 years (1981–1990) for **a** the northern hemisphere, and **b** the southern hemisphere

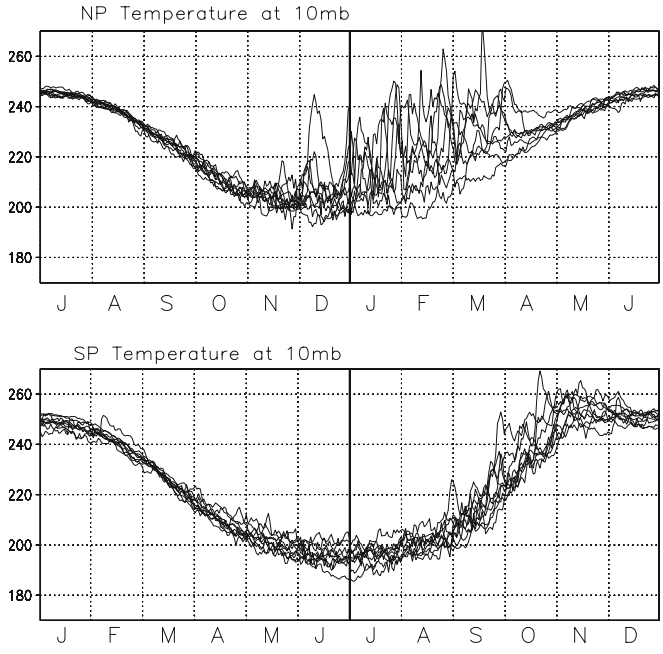


**Fig. 14** Same as Fig. 13 but for the ECMWF reanalysis

We examine the leading EOFs of the model geopotential height variability. For this we use daily geopotential height maps, at 26 pressure levels corresponding to log-pressure altitudes ranging from 0 to 65 km and separated by 2–3 km in the stratosphere and the troposphere. From these maps we subtract the annual cycle and compute, level by level, the EOFs. We apply the same diagnostics to the daily series of geopotential height issued from the ECMWF reanalysis, yielding to one leading EOF pattern for each of the 23 pressure levels of the reanalysis. Figure 15 shows the model leading EOF at three selected levels. The 0 km level EOF-1 is characterized by one negative center of action over the Arctic region, with marked troughs over Greenland, Northern west Siberia, and northern eastern Pacific. It resembles to the same EOF-1 from the reanalysis in Fig. 16a but with some differences. In particular, the trough over Greenland is less pronounced than in the re-analysis data, and the one over northern eastern Pacific more pronounced than in the re-analysis data. In the model, the Arctic negative center of action is associated with an opposing center of action that covers the northern Atlantic and the western Europe. Although too pronounced, this high is also present in the reanalysis EOF-1.

In the stratosphere, the 20 km EOF-1 is dominated by a single negative center of action, nearly exactly centered at the North Pole (Fig. 15b). It is also elongated along the Greenwich meridian. As in the reanalysis dataset (Fig. 16b), it is much broader and zonally symmetric than in the troposphere. Nevertheless, in the model, the EOF-1 pattern is elongated along the Greenwich meridian rather than along Greenland in the reanalysis. At 35 km, the EOF-1 is also centered at the North Pole and is more zonal than the 20 km pattern is. Although it compares with the corresponding pattern from the reanalysis our EOF-1 at 35 km is nevertheless elongated in a direction that is slightly different from that in the reanalysis.

To analyze the vertical development of the model AO, we use next the timeseries of the PC1s normalized at each levels by the standard deviation of the geopotential fields at the same level and after subtraction of the annual cycle. Furthermore, and as we wish to analyze if our model capture the downward propagation of the AO that occurs after sustained stratospheric large scale anomalies, and as those anomalies only occur one or twice each winters (see for instance the North Pole temperature in the model in Fig. 13 or in the reanalysis in Fig. 14), we will isolate the low frequency signals applying to each normalized series of PCs, a 30 day box car average.

The resulting series are presented in Fig. 17. At low frequencies, the large magnitude of the model AO are confined almost entirely to the period October–April. Figure 17 shows that many events are connected in the model from the middle atmosphere to the troposphere. In the model, the AO typically develops around 30–40 km and descents rapidly down to 20 km, it takes little longer timescales to reach the tropopause, and then propagate very rapidly throughout the troposphere (e.g. January 1990). Note that there are a lot of variability in the behavior of the model AO, with some tropospheric events in opposition with those in the stratosphere (e.g. January 1999). Note also that in the model many events develop first near the model top (e.g. around 60 km) and decent throughout the entire atmosphere (e.g. December

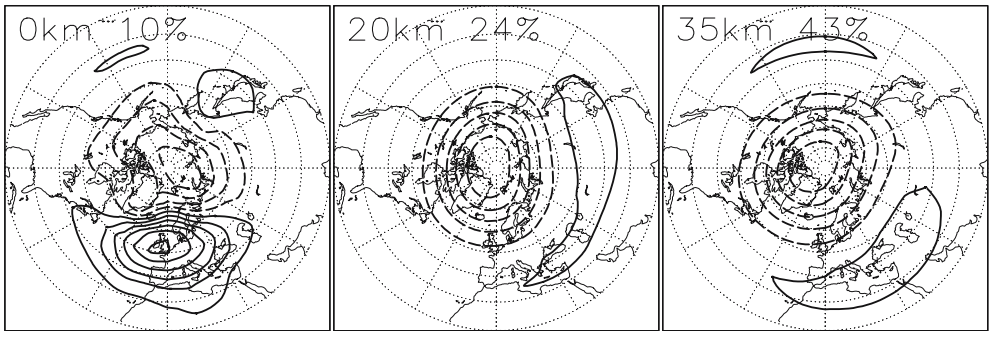


**Fig. 15** Model EOF-1 of the geopotential variability at three selected pressure levels. Altitude and percentage of variance explained at each levels indicated in each panel

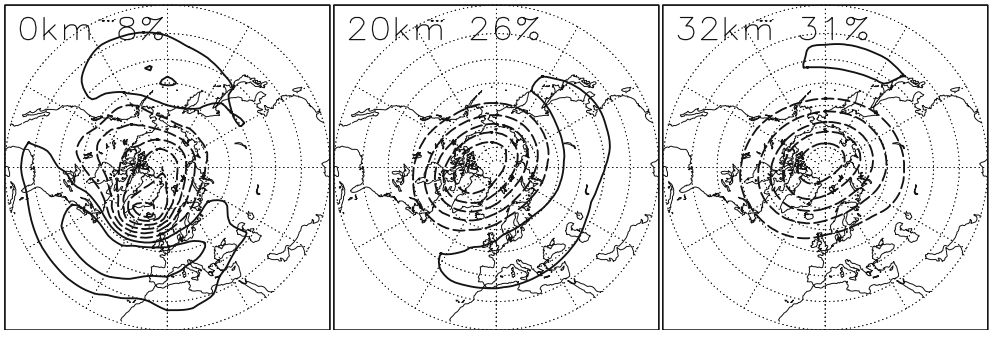


**Fig. 16** Same as Fig. 15 but for the ECMWF reanalysis

1988 to February and March 1989). Note also that in the model, the times where the vortex is very weak around 32 km, often correspond to warming events in mid-winter. More precisely, the North Pole temperature anomaly at 32 km is above 25 K during more than 6 days during the December to February months of the winters 84–85, 86–87, 87–88, 88–89, 89–90, 95–96, 96–97, each of these winters being associated with a weak vortex according to Fig. 17. Conversely, during the same 3-months period, the North Pole temperature anomaly at 32 km is below −20 K during more than 6 days for the strong vortex events seen in the winters 82–83, 91–92, 97–98, 98–99, and 99–00.

It is also important to notice that the relatively slow development of the warmings in the model seen in Fig. 13a, translates into a slower development of the AO signal at all levels. At each levels in the stratosphere, the characteristic timescale for the low-frequency AO signal to change sign in the model is well above 1 month in Fig. 17, while in the reanalysis, this timescale is substantially shorter (Fig. 18).

## 6 Sensitivity to changes in the stratospheric variability

In this section, we follow the approach in Boville (1984) and Norton (2003), and compare the results above to similar results obtained in a simulation where the NH stratosphere climatology is degraded. Here, a different method is nevertheless used, the stratosphere being degraded by enhancing by a factor five the amount of upward propagating OGWs $\beta = 0.5$ instead of 0.9 in the control experiment). Note that compared to Norton (2003) or Boville (1984) we do not damp explicitly the large-scale planetary waves, but rather limit their ability to propagate toward the middle atmosphere by decreasing substantially the zonal-mean zonal wind.

As a result of these modifications the zonal mean zonal wind in Fig. 19a differs substantially in the NH from the control run in Fig. 3a. In particular, the peak of the stratospheric jet in January has been displaced upward and equatorward. In a large zone, between 20 and 30 km, it is below 15 m/s everywhere in the NH, a situation that favors the reflection or the breaking of large scale waves. Although the zonal wind is also affected in the troposphere, the differences are less marked there than in the stratosphere and lower mesosphere. As a consequence, the statistics of the tropospheric variability (i.e the mean and the standard deviations of the geopotential at 700 hPa) are not very different from the control case in Fig. 7 (not shown). The center of action of winter variability over north eastern Pacific and north eastern Atlantic are nevertheless a few percent less intense than in the control case.

Although the model tropospheric variability in the strong drag case is still realistic, the much reduced winds due to the OGWs in the lower stratosphere result in reduced planetary waves in the stratosphere in NH winter (for the first planetary wave, see Fig. 19c, d, e). As a consequence the variability of the zonal mean of the geopotential height is much reduced as well (Fig. 19b), and the late winter variations of the North Pole temperature in Fig. 19f are much smaller than in the control run (Fig. 13a). These variations are also of shorter timescales, indicating that the timescale of the warmings in the model is dynamically controlled.

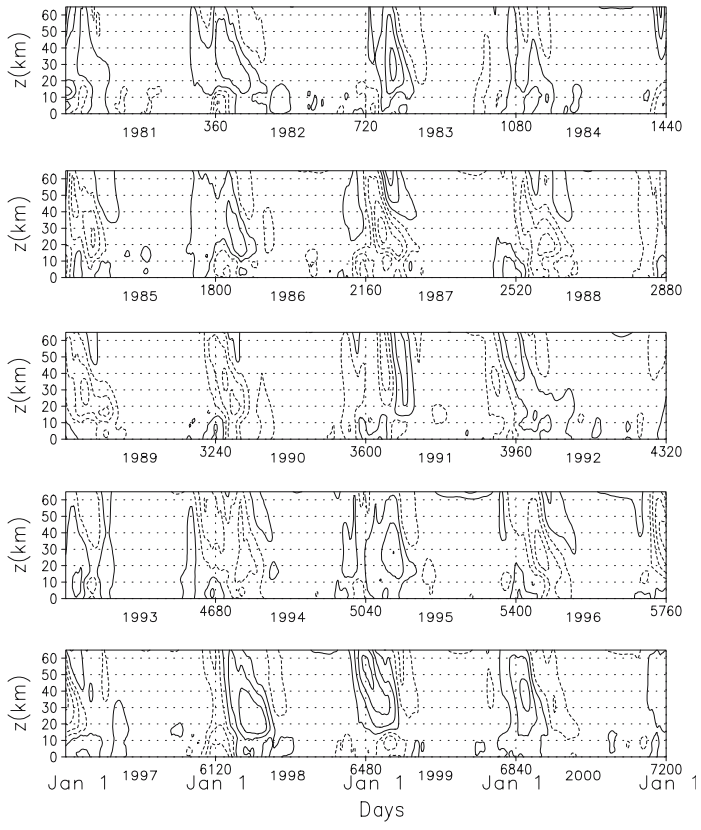


**Fig. 17** PC-1 time series from the model. At each level, the PC series are normalized by the standard deviation of the geopotential at that level. All resulting series are also filtered by a 30-day box car average. Negative values (*dashed lines*) correspond to a weak (warm) polar vortex

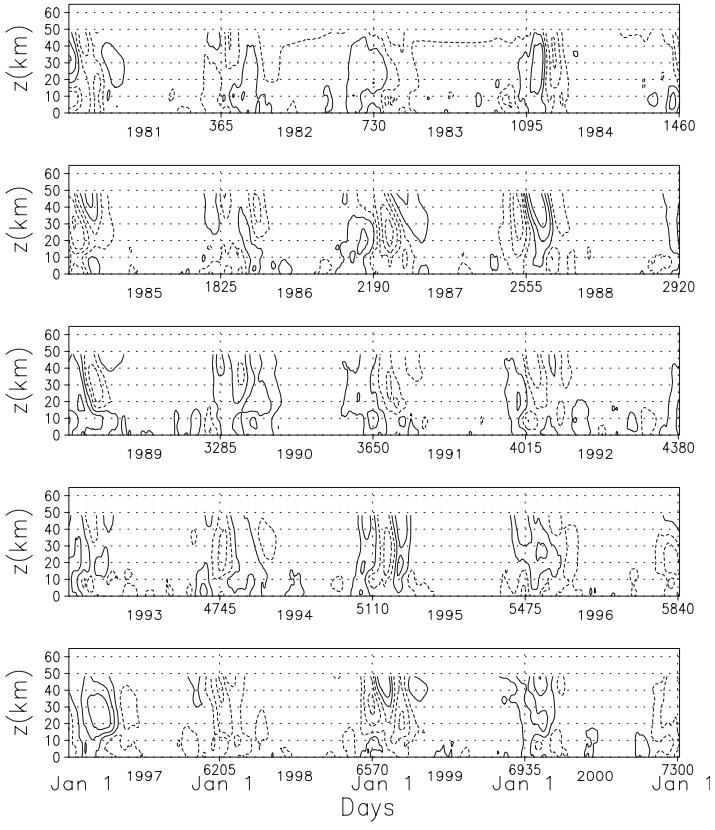


**Fig. 18** Same as Fig. 17 but from the ECMWF reanalysis

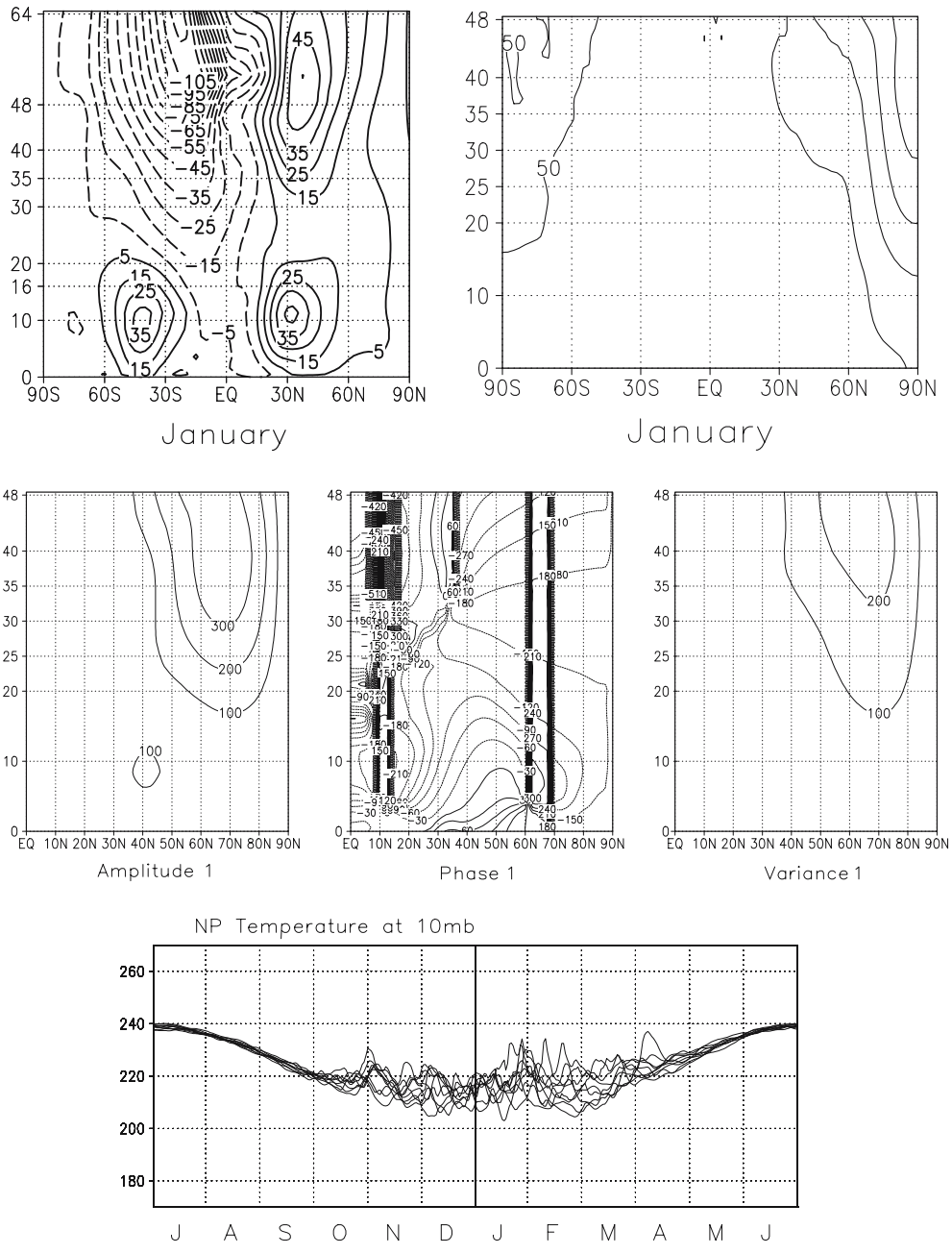


**Fig. 19** Some diagnostics from the simulation with strong orographic gravity waves. **a** Zonal mean of the zonal wind in January (as Fig. 3a); **b** standard deviation of the zonal mean of the geopotential height in January (as Fig. 11a); **c–e** January planetary wave number one diagnostics (as Fig. 9a, b, c); **f** North Pole temperatures (as Fig. 13a)

Despite those differences, the leading EOFs of NH variability in the strong drag case (not shown) are not very far from those in the control run. The most noticeable difference is that above 15 km, the leading EOFs represent much less variance than in the control run (17% at 20 km and 24% at 35 km, instead of 24% and 43% respectively in the control run). The temporal evolution of the normalized PC∼1, is presented in Fig. 20. Clearly, the model has lost a good part of the stratosphere–troposphere AO connections seen in the control run in Fig. 17. More precisely, there are a lot of dates (i.e. much more than in the control run and near each winters), where a stratospheric anomaly develops and decreases without being related to a corresponding anomaly in the troposphere (e.g. Jan–Feb 1981, Jan–Feb 1983, Jan–Feb 1985, ...). There are also periods where substantial anomalies descend from the model lower mesosphere to the lower-middle stratosphere but do not reach the tropopause (Jan–Feb 1984, Jan–Feb 1990, Jan–Feb 1995, and Jan–Feb 1998). This last behavior was near absent in the control simulation and rather rare in the reanalysis (Fig. 18).

The fact that the downward propagation of the AO can lead to increase the predictability of the surface AO in the model is illustrated in Fig. 21. Following Norton (2003), it presents the autocorrelation of the PC-1 values at 10 and 1,000 hPa from the control run (thick solid), strong OGWs (thick dashed), from the reanalysis data

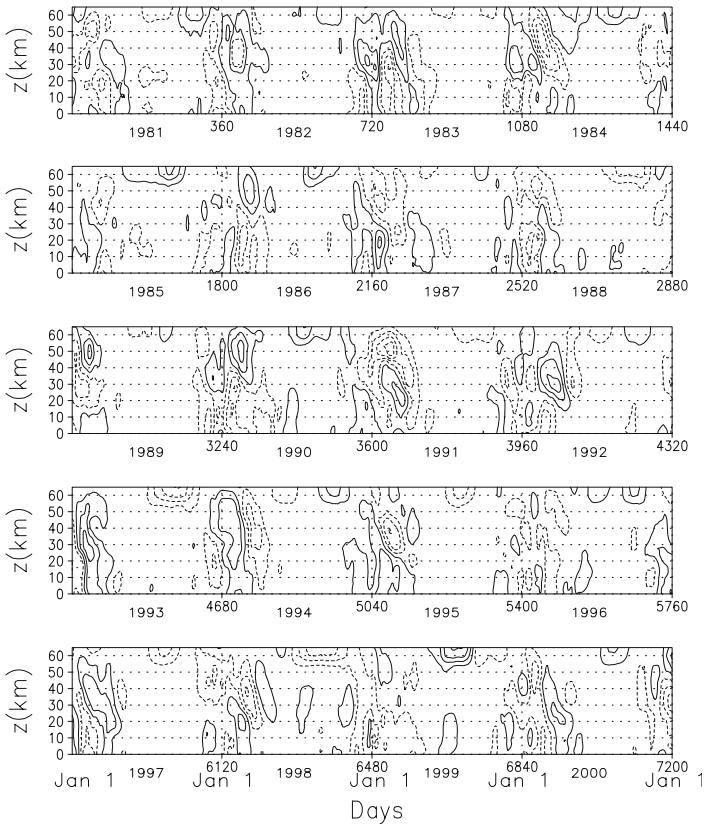


**Fig. 20** Same as Fig. 17 but with strong orographic gravity waves

(thick dotted), and from the routinely used tropospheric version of the model. At the two levels, the control run has a slower decay than the strong OGWs run.

At 10 hPa and at all lags, the temporal decorrelation of the AO in the control run is much more realistic than in the strong OGWs case (Fig. 20a). Nevertheless it is nearly always larger than in the reanalysis (dots), indicating that the stratospheric low frequency variability evolves more slowly in the model than it does in the observation. This behavior could have been noticed already in the discussion of Fig. 13a, where it is apparent that the warming events in the model, last substantially longer than in the reanalysis in Fig. 14a.

At 1,000 hPa and at small lag (i.e. for lags below 10 days), all runs underestimate the decorrelation of the AO. Accordingly, it is not surprising to find the autocorrelation in the strong OGW run nearer the reanalysis than is the control run. At longer lags (i.e., between 20 and 30 days) the autocorrelation of the 1,000 hPa AO in the control run becomes nearer the reanalysis than in the strong OGWs run. Nevertheless, this apparent superiority of the control run should be considered with

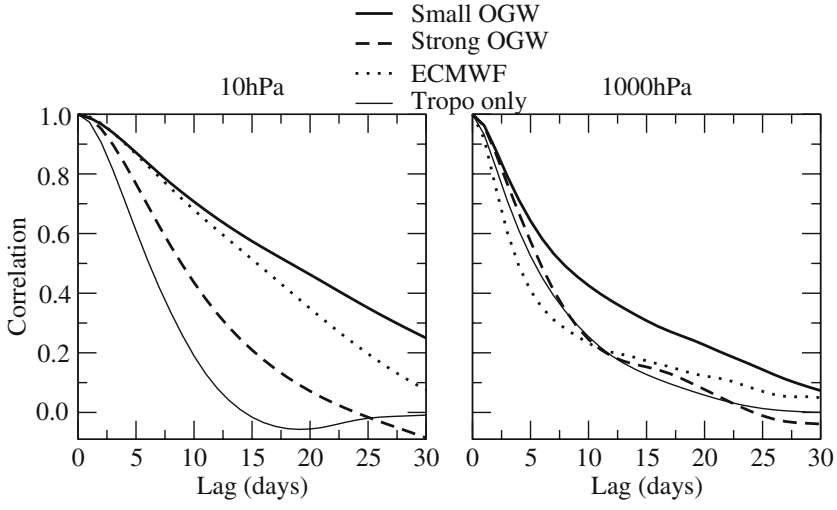


**Fig. 21** Autocorrelation of the PC-1 at 10 hPa and 1,000 hPa. *Solid lines* are for the control run, *dashed lines* are for the strong orographic gravity waves run and the *dotted lines* are for the ECMWF reanalysis

caution, the reanalysis AO being affected by low frequency changes in external forcings (i.e., due to intra-seasonal changes in SST for instance) that are absent in our simulations.

It is also of interest to note that the tropospheric variability in our strong OGWs drag case is representative of that in the tropospheric version of the model (19 levels with only four in the stratosphere, same horizontal resolution). Accordingly, the decorrelation of the AO at 1,000 hPa in this operational version (thin line in Fig. 21b) is rather near that of the strong OGWs case, and closer to reality than the control run is. Although this is not much surprising, all parameters in the tropospheric model being tuned for years to adjust its climatology, it happens that the introduction of the stratosphere leads to increase too much the surface AO persistence and predictability.

## 7 Summary and conclusions

This paper has presented some aspects of the radiative dynamical climatology and of the variability of the first stratospheric version of the atmospheric general circulation model LMDz. Following earlier developments, this model has a realistic tropospheric climate (Lott 1999; Li 1999), and has its higher level near above 65 km, a conventional value for stratospheric GCMs. The first motivation of this work was to provide a first reference model climatology as a point of comparison for future model improvements.

Our climatologies have been obtained from a 20 year reference simulation, which is long enough to analyze quantitatively the model ability to simulate the mean climate and its interannual variability. The monthly mean fields presented in Sect. 3.1 show that the model captures the basic features of the stratosphere temperature and distribution. There is nevertheless a cold bias in the wintertime stratosphere, which is present in both poles and despite the fact that the model includes parameterizations of orographic and non-orographic gravity waves. Although these biases could have been reduced further by enhancing the strength of the gravity waves in these parameterizations, we have not chosen that strategy because the GWs parameterizations also affect indirectly the planetary wave activity, which we wanted to stay close to reality as well. The transformed Eulerian mean meridional circulation has been examined in Sect. 3.2, and exhibits the expected features.

Diagnostics of the model's ability to simulate the tropospheric steady planetary waves and the tropospheric low-frequency variability are presented in Sect. 4.1. Their realism is in good part due to the SSO parameterization in Lott (1999) and is comparable to that in the routinely used tropospheric version of the model (Lott 1999). This demonstrates that the introduction of a stratosphere does not degrade the model simulation of the tropospheric climate. It also confirms that the model troposphere can force the large-scale planetary waves that largely control the large-scale stratosphere dynamics.

Some diagnostics of the stratospheric variability are then given in Sect. 4.2. They show that the model reproduces qualitatively well the planetary waves in the winter NH, with a slight tendency to overestimate their amplitude and variability. Although not shown, the same results hold for the other months. As a result of the interaction of these waves with the zonal flow the variability of the zonal mean geopotential height is also well reproduced although slightly overestimated by the model. As a consequence, the 10 hPa temperature variations at both poles are also realistic in amplitude, with the model producing stratospheric warming in the northern hemisphere in late winter and early spring. In contradiction with the observations, it does not seem to produce warmings in December, and the temporal variations of the North-Pole temperature also seems to occur on longer timescales than they do in the reanalysis.

In order to evaluate the dynamical connections between the large-scale stratospheric circulation and the tropospheric variability in the model, an analysis of the model AO has been done in Sect. 5. Although there are some differences between the patterns of the model AO and the observed ones, this mode of variability seems to connect the stratospheric dynamics and the tropospheric one at low intra-seasonal frequencies. There are times where the AO signal in the stratosphere precedes that in the troposphere.

A sensitivity experiment was then carried out, where the OGWs that reach the stratosphere are exaggerated (Sect. 6). This weakens the stratospheric jet in the winter NH lower stratosphere and shifts it equatorward in the whole stratosphere. This zonal mean flow change reduces the planetary wave activity in the stratosphere, prevents stratospheric warmings and reduces the zonal mean stratospheric variability. Still, in this experiment, the variability at all levels stays dominated by AO-like patterns that resemble those in the control run. On top of that, the tropospheric variability is not much different from that in the control run. Despite these two similarities, it happens that the downward propagation of the AO is in good part lost, and the surface AO is much less persistent. These results suggest that the AO propagation from the stratosphere to the troposphere is one of the dynamical factors that increase the persistence of the surface AO.

Nevertheless, when we compare the model with the reanalysis, we find that the control run overestimates the surface AO persistence. In this respect, the run with a degraded stratospheric variability is much more realistic. Indeed, it behaves very much like the routinely used 19-levels tropospheric version of the model. Although this defect of the stratospheric version may be related to the fact that our stratospheric variability is too slow, it also indicates that the introduction of the stratosphere in a

particular GCM may lead to overestimate its role on the tropospheric climate.

On the one hand, these last results should not be interpreted in the sense that the extension to the stratosphere degrades the GCMs that are developed to study the climate and its future changes. Indeed, all the parameters of the routinely used tropospheric version of LMDz have been tuned in the past to produce a realistic tropospheric climate. So it is not surprising that the extension to the stratosphere done here by changing only few of these parameters has a negative impact. Furthermore, the impact we see here is rather realistic, in the sense that there are large evidences these days that the AO persistence is increased by the stratospheric dynamics. In this sense, and as the central purpose of this paper is to validate our model, we find positive that our model goes in the right direction regarding this particular diagnostics. On the other hand, these results indicate that the introduction of the stratosphere call for a new adjustment of the model parameters that control the low-frequency variability in the NH midlatitudes. One of the most important among these parameters is probably the horizontal resolution.

## References


Andrews DG, Holton JR, Leovy CB (1987) Middle atmosphere dynamics. Academic Press, 489pp

Baldwin MP, Dunkerton TJ (1999) Propagation of the arctic oscillation from the stratosphere to the troposphere. J Geophys Res 104: 30,937–30,946

Beagley SR, de Grandpré J, Koshyk JN, McFarlane NA, Shepherd TG (1997) Radiative dynamical climatology of the first generation Canadian middle atmosphere model. Atmosphere-Ocean 35:293–331

Blackmon ML (1976) A climatological study of the 500 mb geopotential height of the northern hemisphere. J Atmos Sci 33:1607–1623

Bony S, Dufresne J-L, LeTreut H, Morcrette J-J, Senior C (2004) On dynamic and thermodynamic components of cloud changes. Clim Dynam 22:71–86

Boville BA (1984) The influence of the polar night jet on the tropospheric circulation in a GCM. J Atmos Sci 41:1132–1142

Boville BA (1995) Middle atmosphere version of CCM2 (MACCM2): annual cycle and interannual variability. J Geophys Res 100:9017–9039

Butchart N, Austin J (1998) Middle atmosphere climatogies from the troposphere-stratosphere configuration of the UKMO's Unified Model. J Atmos Sci 55:2782–2809

Charney JG, Drazin PG (1961) Propagation of planetary-scale disturbances from the lower into the upper atmosphere. J Geophys Res 66:83–109

Christiansen B (2001) Downward propagation of zonal mean wind anomalies from the stratosphere to the troposphere: model and reanalysis. J Geophys Res 106:27,307–27,322

Déqué M, Dreverton C, Braun A, Cariolle D (1994) The ARPEGE/IFS atmosphere model: a contribution to the French community climate modelling. Clim Dynam 10:249–266

Fels SB, Mahlman JD, Scharkopf MD, Sinclait RW (1980) Stratospheric sensitivity to perturbations in ozone and carbon dioxide. J Atmos Sci 37:2265–2297

Fleming EL, Chandra S, Barnett JJ, Corney M (1990) Zonal mean temperature, pressure, zonal wind and geopotential height as a function of latitude. Adv Spa Res 10(12):11–59

Fortuin JPF, Kelder H (1998) An ozone climatology base on ozonesonde and satellite measurements. J Geophys Res 103: 31,709–31,734

Hamilton K, Wilson RJ, Mahlman JD, Umscheid LF (1995) Climatology of the SKYHI troposphere-stratosphere-meseophere general circulation model. J Atmos Sci 52:5–43

Hauglustaine DA, Hourdin F, Jourdain L, Filiberti M-A, Walters S, Lamarque J-F, Holland EA (2004) Interactive chemistry in the laboratoire de meteorologie dynamique general circulation model: description and background tropospheric chemistry evaluation. J Geophys Res 109(D4):4314

Hines CO (1997a) Doppler spread parameterization of gravity wave momentum deposit in the middle atmosphere. Part I: basic formulation. J Atmos Solar Terr Phys 59:371–386

Hines CO (1997b) Doppler spread parameterization of gravity wave momentum deposit in the middle atmosphere. Part II: broad and quasi monochromatic spectra and implementation. J Atmos Solar Terr Phys 59:387–400

Hoskins B J, Hsu HH, James IN, Masutani M, Sardeshmuck PD, White GH (1989) Diagnostics of the global atmospheric circulation based on ECMWF analysis 1979—1989. WCRP/WMO technical document 326:217

Hourdin F, Couvreux F, Menut L (2002) Parameterisation of the dry convective boundary layer based on a mass flux representation of thermals. J Atmos Sci 59:1105–1123

Krinner G, Genthon C (2003) Tropospheric transport of continental tracers towards Antarctica under varying climatic conditions. Tellus 53:54–70

Langematz U, Pawson S (1997) The Berlin troposphere-stratosphere-mesosphere GCM: climatology and forcing mechanisms, Q J R Meteor Soc 123:1075–1096

Li L (1999) Ensemble atmospheric GCM simulation of climate interannual variability from 1979 to 1994. J Climate 12:986–1001

Lott F (1999) Alleviation of stationary biases in a GCM through a mountain drag parametrization scheme and a simple representation of mountain lift forces. Mon Weather Rev 127:788–801

Lott F, Miller M (1997) A new subgrid scale orographic drag parameterization; its testing in the ECMWF model. Q J R Meteor Soc 123:101–127

Manzini E, McFarlane NA (1998) The effect of varying the source spectrum of a gravity wave parameterization in a middle atmosphere general circulation model. J Geophys Res 103:31,523–31,539

Manzini E, McFarlane NA, McLandress C (1997) Impact of the Doppler spread parameterization on the simulation of the middle atmosphere circulation using the MA/ECHAM4 general circulation model. J Geophys Res 102:25,751–25,762

Morcrette JJ (1991) Radiation and cloud radiative properties in the European center for medium range weather forecasting system. J Geophys Res 96:9121–9132

Norton WA (2003) Sensitivity of northern hemisphere surface climate to simulation of the stratospheric polar vortex. Geophys Res Lett 30:1627. DOI 10.1029/2003GL0116958

Pawson S, Coauthors (2000) The GCM-reality intercomparison for SPARC (GRIPS): scientific issues and initial results. Bull Amer Meteor Soc 81:781–796

Perlwitz J, Harnick N (2003) Observational evidence of a stratospheric influence on the troposphere by planetary wave reflection. J Clim 16:3011–3026

Polvani LM, Kushner PJ (2002) Tropospheric response to stratospheric perturbations in a relatively simple general circulation model. Geophys Res Lett 29:1114. DOI 10.1029/2001GL014284

Preisendorfer R W (1988) Principal component analysis in meteorology and oceanography. Elsevier Science, New-York, pp 425

Quaas J, Boucher O, Bréon F-M (2004) Aerosol indirect effects in polder satellite data and the laboratoire de meteorologie dynamique-zoom (lmdz) general circulation model. J Geophys Res 109:D08205. DOI 10.1029/2003JD004317

Reddy MS, Boucher O (2004) A study of the global cycle of carbonaceous aerosols in the lmdzt general circulation model, J Geophys Res 109:D14202. DOI 10.1029/2003JD004048

Rind D, Scuozzo R, Balachandran NK, Lacis A, Russel G (1988) The GISS global climate-middle atmosphere model. Part 1: model structure and climatology. J Atmos Sci 45:329–370

Sadourny R (1975) The dynamics of finite difference models of the shallow water equations. J Atmos Sci 32:680–689

Sawyer JS (1976) Observational characteristics of atmospheric fluctuations with a time scale of a month. Q J R Meteorol Soc 96:610–625

Shepherd TG, Semeniuk K, Koshyk JN (1996) Sponge layer feedbacks in middle atmosphere models. J Geophys Res 101:23,447–23,464

Simmons AJ, Gibson JK (2000) The ERA-40 project plan. ERA-40 Project Report Series 1:63p

Song Y, Robinson WA (2004) Dynamical mechanisms for stratospheric influences on the troposphere. J Atmos Sci 61:1711–1725

Thompson DW, Wallace JM (1998) The arctic oscillation signature in the wintertime geopotential height and temperature fields. Geophys Res Lett 25:1297–1300

Tiedtke M (1989) A comprehensive mass flux scheme for cumulus parameterization in large-scale models. Mon Weather Rev 117:1779–1800